Article

Wireless Nanobioelectronics for Electrical Intracellular Sensing

Paola Sanjuan-Alberte, Frankie James Rawson, Akhil Jain, Andie Shaw, Sidahmed Abayzeed, Rafael Rafael Fuentes Dominguez, Maria Elisa Alea-Reyes, Matt Clark, Morgan R. Alexander, Richard J.M. Hague, and Lluisa Perez-Garcia

ACS Appl. Nano Mater., **Just Accepted Manuscript** • DOI: 10.1021/acsanm.9b01374 • Publication Date (Web): 05 Sep 2019

Wireless Nanobioelectronics for Electrical Intracellular Sensing

*Paola Sanjuan-Alberte[a,b], Akhil Jain[a], Andie J Shaw [a], Sidahmed A Abayzeed[a], Rafael Fuentes Domínguez[c], María E Alea-Reyes[d], Matt Clark[c], Morgan R Alexander[e], Richard JM Hague[b], Lluïsa Pérez-García[e], Frankie J Rawson[a]**

[a] Regenerative Medicine and Cellular Therapies, School of Pharmacy, University of Nottingham, Nottingham, NG7 2RD UK

[b] Centre for Additive Manufacturing, Faculty of Engineering, University of Nottingham, Nottingham, NG7 2RD, UK

[c] Optics and Photonics Research Group, Faculty of Engineering, University of Nottingham, Nottingham, NG7 2RD, UK

[d] Departament de Farmacologia, Toxicologia i Química Terapèutica, Universitat de Barcelona, Avda. Joan XXIII 27-31, 08028 Barcelona, Spain

[e] Advanced Materials and Healthcare Technologies, School of Pharmacy, University of Nottingham, Nottingham, NG7 2RD, UK

Keywords: wireless bioelectronics, nanoelectrochemistry, intracellular sensing, dark field microscopy, zinc porphyrin

Abstract

For the field of bioelectronics to make an impact on healthcare, there is an urgent requirement for the development of "wireless" electronic systems to enable modulation of chemistry inside of cells. Herein we report on an intracellular wireless electronic communication system. This is based on modulating the electrochemistry on gold nanoparticles without the nanoparticles having any physical electrical connection to a power supply at relatively low externally applied potentials. The system is made functional by modifying water soluble gold nanoparticles (ws-AuNPs) with a Zn(II)meso-tetrakis(4-carboxylateyphenyl)porphyrin sodium salt (Na-ZnTCPP). Na-ZnTCPP modified ws-AuNPs are taken up by cells and are shown to be non-cytotoxic. It is demonstrated that the redox state of the Zn-porphyrin modified gold nanoparticles is controlled and a fluorescent output can be used to measure this during the application of an external electrical potential. When the porphyrin modified nanoparticles were located intracellularly and external potentials were applied the same effect was observed. This provides an attractive "wireless" approach to develop bioelectronic devices for modulating and sensing cellular behaviour.

Introduction

The field of bioelectronic medicine offers a new paradigm in therapeutic intervention[1-3]. The technology is in its infancy, but relies on the ability to merge electronic devices with biology effectively[4]. The key challenge in advancing the field further is to develop new non-invasive methods to both electrically sense and actuate cell behaviour. Our group[5-7] and others[8-11] have

pioneered new methods for electrically communicating with the internal environment of a cell via use of nanowire electrodes. However, these methods tend to be invasive in nature as they necessarily have to pierce the plasma membrane which can lead to cell perturbations[12-13]. In addition, these electrodes require physical electrical connectivity from inside of the cells to the outside, thus hindering their use in more complex biological environments. Therefore, an approach to address these issues is to develop novel wireless electronic systems for the development of intracellular sensors and actuators. The development of novel bioelectronics using such a wireless-electronic approach may subsequently enable significant advancements in the ability to use intracellular electronics to facilitate cell communication and actuation[14]. Therefore, the aim of this work was to develop a new bioelectronic approach for sensing electrical changes in response to the application of an externally applied voltage inside biological cells, thereby offering the first example of a wireless electronic tool to modulate redox chemistry at conductive nanoparticles[15]. This may then be used in future to develop tools to modulate chemistry inside of cells using an external electric field.

The work undertaken was inspired by the fields of bipolar electrochemistry and drug delivery. Bipolar electrochemistry (also known as wireless electrochemistry) relies on placing a conductive particle between feeder electrodes, which have a potential difference placed across them. This causes the conductive particle to polarize and in doing so, causes a potential difference between the electrolyte and poles of the particle, consequently providing the thermodynamic driving force required to modulate redox reactions[16-18]. However, the previous example of performing bipolar electrochemistry at a nanoparticle required voltages that were in the range of kV[19] as smaller particles require higher potentials according to this theory[20], this was thought to preclude its use

in biology. To emphasize, no bipolar-electrochemistry at nanoparticles has been shown to occur in the voltage window of 1-100s of volts. Nanoparticles have been used as drug delivery vectors for many years. One mechanism that has been used to deliver payloads to cells are conductive gold nanoparticles[21]. These have been shown to be internalized into cells in a non-invasive manner, are biocompatible[22] and have been extensively reviewed[23-26]. Their use in drug delivery research is widespread because the surface of gold is readily adaptable to surface chemistry modifications, facilitating functionalization of the nanoparticle with drugs.

Our strategy for developing a wireless bioelectronic tool included three key steps: (1) Firstly, we established evidence that relatively low potentials caused wireless electrical induced redox effects at 'naked' or unmodified gold nanoparticles (u-AuNPs) (**Figure 1a**). Electrochemical deposition of palladium was modulated in a wireless manner on the gold surface. (2) Development of a dark field microscopy tool was undertaken in order to provide direct evidence that u-AuNPs could be used as electronic sensors at low voltages. This was achieved by imaging the electrical surface charge via plasmonic effects on the gold nanoparticles. (3) Development of intracellular nanosensors by synthesizing of water soluble gold nanoparticles (ws-AuNPs) (**Figure 1b**) modified with a Zn(II)meso-tetrakis(4-carboxylateyphenyl)porphyrin sodium salt (Na-ZnTCPP) (**Figure 1c**) Chemical structures of the different components can be seen in **Figure 1d-f**. (4) Study of changes in fluorescence when an electronic input was applied. These particles were incubated with Chinese Hamster Ovary (CHO) cells and were taken up inside. We proved that the modified gold nanoparticles could act as electrical reporters, when applying an external electric field, by modulating the Na-ZnTCPP, which could be optically followed by fluorescence microscopy.

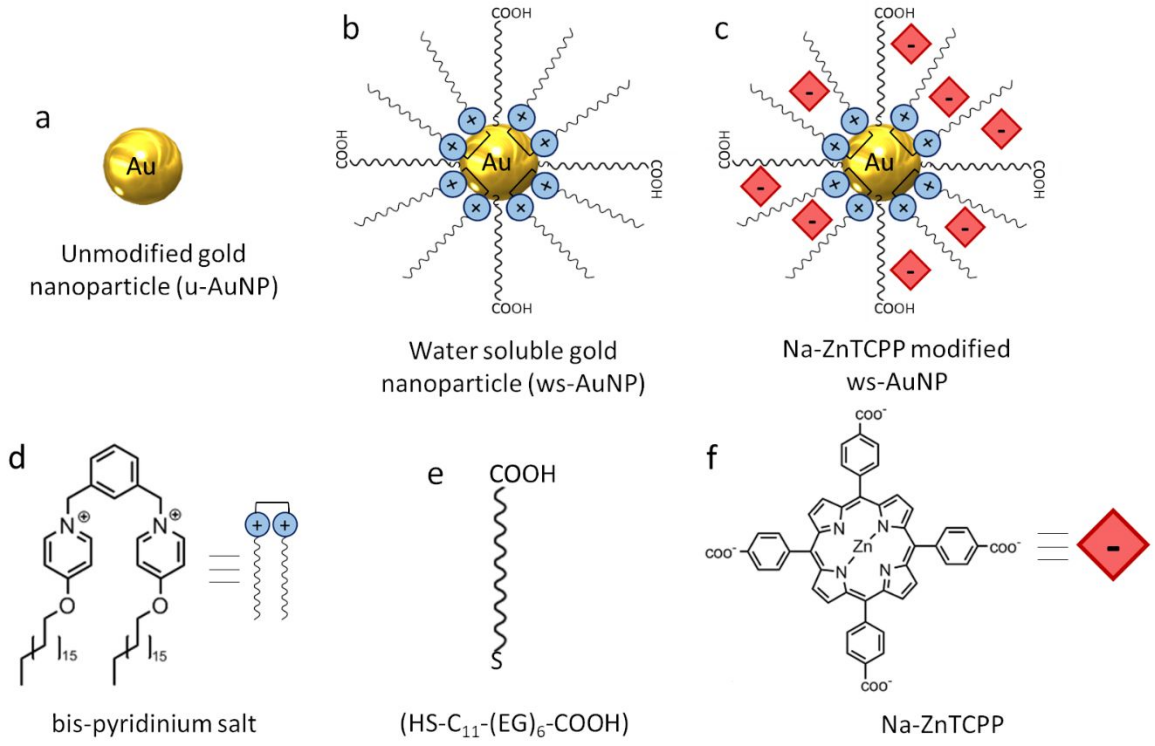

Figure 1. Schematic representation of a) unmodified gold nanoparticle (u-AuNP), b) water soluble gold nanopatrticle (ws-AuNP), c) Zn(II)meso-tetrakis(4-carboxyphenyl)porphyrin sodium salt (Na-ZnTCPP) modified ws-AuNP; and chemical composition of d) bis-pyridinium salt, e) α-thio-ω-carboxy-polyethylene glycol and f) Na-ZnTCPP[27].

Results and discussion

The goal of this work was to develop a new wireless nano-electronic communication system inside of cells. The work was in part motivated by bipolar electrochemistry for which most reported cases have been achieved at the macro/micro-scale[16, 18]. Therefore, to extend this approach to the dimensions required for intracellular measurement, we initially set out to investigate the effect of placing 50 nm sized unmodified gold nanoparticles (u-AuNPs, PBS stabilized u-AUNP were commercially purchased) between electrodes after application of a potential difference. This was

done in the presence and absence of 1 mM palladium chloride ($PdCl_2$). Potentials were applied using an inkjet printed electrochemical cell consisting of two gold feeder electrodes with a separation of 210 μm and a silver/silver chloride pseudo-reference electrode (Figure S1), which was characterized using cyclic voltammetry prior to use (Figure S2).

We envisaged that the u-AuNPs would align in the electric field which would cause them to polarize thereby causing a potential difference between the poles. This potential difference could then provide the thermodynamic driving force to reduce $Pd^{+2}_{(aq)}$ thereby depositing $Pd^{0}_{(s)}$ on the u-AuNPs as depicted in **Figure 2a**. 'Naked' u-AuNPs are needed in this case as surfaces need to be exposed to the solution in order for the electrodeposition to take place at the Au surface. After applying the electrical input of 10 V at the varying times of 0, 1, 5 and 15 minutes, we collected the solutions of u-AuNPs and characterized the size of the particles by dynamic light scattering (DLS). The u-AuNPs in the solution that were not exposed to the potential difference of 10 V had a size of 59.58 ± 0.35 nm. In the presence of the $PdCl_2$ the size increased to 108.3 ± 1.3 nm. After one minute of applying 10 V there was no difference in the size of the nanoparticles when compared to those that were not exposed to a potential difference of 10 V (**Figure 2b**). However, after exposure to the potential difference for 5 and 15 minutes there was a significant difference in size of the nanoparticles with an increase in size to approximately 745.5 ± 51.8 nm and 718.0 ± 38.4 nm, respectively. We suggest that this difference in size occurs because the reduction of the palladium and oxidation of the chloride ions occurs at the surface of u-AuNPs (**Figure 2a**), leading to deposition of $Pd^{0}_{(s)}$ nanoparticles (**Figure 2b**) and resulting in larger particles.

We further investigated the size and elemental composition of the particles to provide additional evidence of the mechanism resulting in the increase in size via transmission electron microscopy (TEM). Consequently, we placed the different samples into a holey carbon grid and performed TEM investigations, coupled with Energy Dispersive X-ray (EDX) on the u-AuNPs that had the $Pd_{(s)}$ deposited. Individual particles with Pd deposits were observed (**Figure 2c**), and elemental EDX spectra confirmed that there was a distribution of $Pd_{(s)}$ and $Au_{(s)}$ suggesting the application of an electric field resulted in the wireless electrodeposition of $Pd_{(s)}$ on the gold (**Figure S3**). This effect was not observed in the unstimulated samples containing u-AuNPs + 1 mM $PdCl_2$ (**Figure S4**). This was also further supported by scanning electron microscopy (SEM) and images of big aggregates showing the same behavior (**Figure S5**). This finding demonstrates the feasibility to electrically mediate redox reactions at the surface of the gold nanoparticles without the need for direct electrical wiring of the gold nanoparticles.

The discrepancy between the sizes of particle observed when analyzing with DLS and those analyzed with SEM (700 nm measured by DLS vs 10 μm agglomerates observed by SEM, Figure S5) can be attributed to differences in preparation of samples. In the DLS experiments the nanoparticles were in solution and in the SEM they were dried, which can cause agglomeration of the particles. The increase in size of the gold nanoparticles only occurred when applying an electric field and a potential difference between the feeder electrodes in the presence of the $PdCl_2$, indicating that applying the potential difference between the feeder electrodes induces the wireless modulation of redox effects at the gold nanoparticle solution interface. This redox mediated deposition of $Pd_{(s)}$ at gold nanoparticles displayed some unique properties since the deposition was occurring at relatively low potentials of 10 V compared to the other electrical induced redox effect

investigated at the nanoscale, which required application of kV[19]. However, we tentatively suggest it could be due to plasmon effects which lower the energetics associated with electronically modulating the redox reactions[28-29].

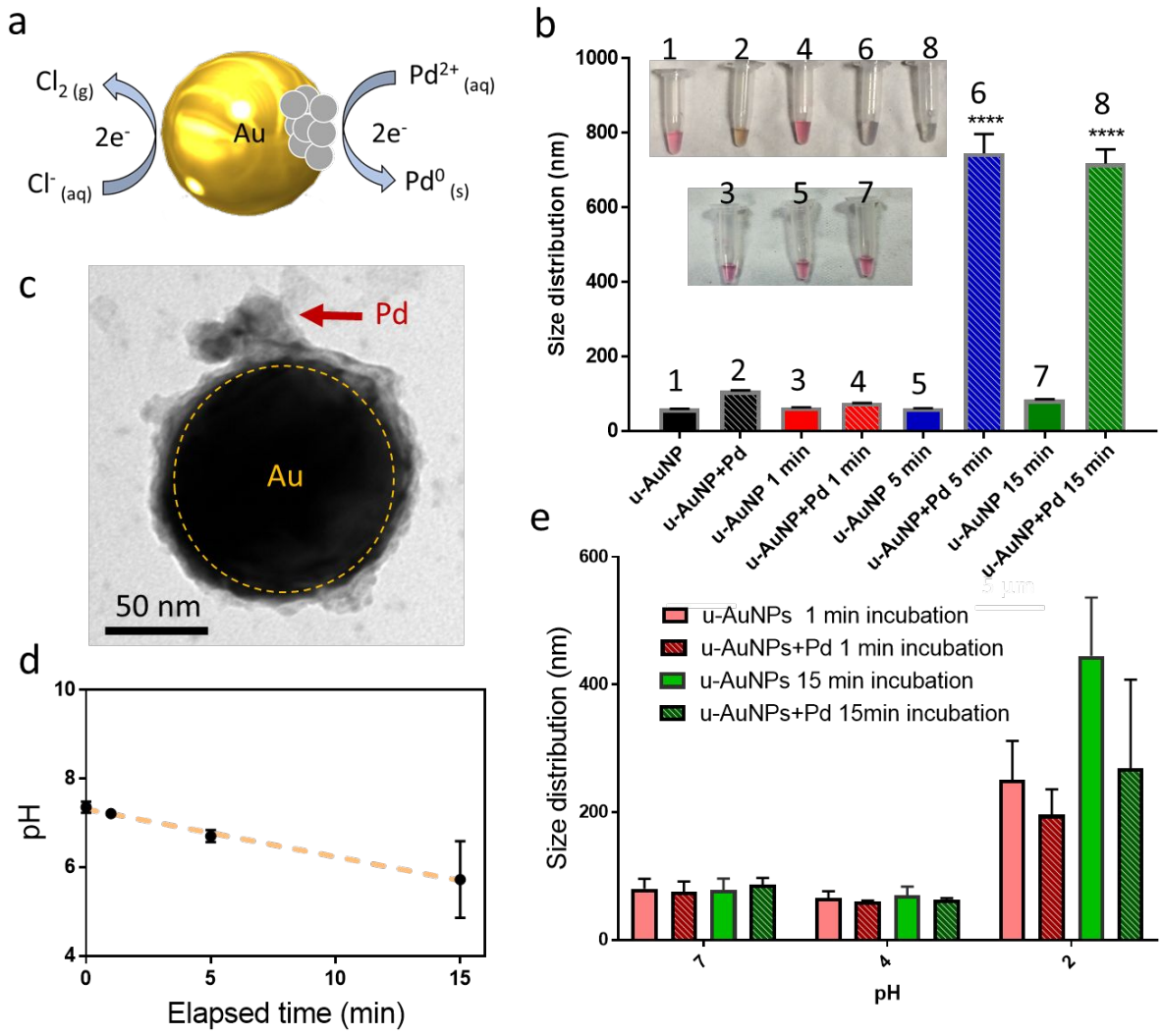

Figure 2. (a) Diagrammatic representation of proposed electrical induced reaction in u-AuNPs. 10 V vs $Ag/AgCl_2$ was applied to solutions of u-AuNPs and u-AuNPs in the presence of 1 mM $PdCl_2$ for 1, 5 and 15 min and the size of u-AuNPs was (b) measured by DLS (n=3: SD). (c) TEM image of Pd deposits on individual u-AuNPs (arrow) after the application of 10 V for 10 minutes.

(d) Effect of applying 10 V between 0 and 15 minutes on the pH of the solution. (e) Dynamic light scatter study of AuNP in the presence and absence of 1 mM $PdCl_2$ on buffer solutions at either pH 7, 4, or 2. (n=3 ; SD)

At the magnitude of the potential applied, water electrolysis would occur at the feeder electrodes and therefore protons would be generated; we therefore sought to establish the effect of the production of proton on $Pd_{(s)}$ deposition on the $Au_{(s)}$ to ensure the electronic effect was not an indirect one mediated by electrolysis of water and proton production. Accordingly, we measured the pH of the solution containing u-AuNPs and $PdCl_2$ at 0, 1, 5 and 15 minutes after applying a potential difference of 10 V between the feeder electrodes. It was demonstrated that there was a linear correlation between the pH of the solution and the time that potentials were applied (R^2 = 0.995), i.e. with a change in pH from 7.36 ± 0.13 at t = 0 to 5.72 ± 0.87 after 15 minutes of application of 10 V (**Figure 2d**).

To rule out the possibility that aggregation of u-AuNPs was being mediated by changes in the pH via this proton generation, u-AuNPs were incubated in the presence and absence of $PdCl_2$ (1 mM) in buffer solutions at pH 2, 4 and 7 for 1 and 15 minutes (**Figure 2e**). The size of the nanoparticle was analysed by DLS showing that at pH 7 and 4 there was no significant change in size for any of the u-AuNPs solutions. However, at pH 2 there was a significant increase in the size of u-AuNPs confirming such acidic pH could induce aggregation of the nanoparticles. Nevertheless, as the pH recorded with an application of potential for 15 minutes only resulted in a reduction of the pH to 5.72, the premise that protons play any part in particle aggregation upon Pd^{2+} reduction and the increases in size of the nanoparticles can be rejected. Therefore, this

provides further evidence that the change in size of the nanoparticle on application of an electrical input occurs due to u-AuNPs being directly affected by the electrical input, resulting in wireless redox induced communication with the nanoparticles via Pd^{2+} reduction.

Our observations suggested that we could wirelessly drive redox chemistry via the application of an electrical field at unreported low voltage difference that was orders of magnitude lower to that reported at other nanostructures, such as carbon nanotubes (CNTs)[19]. To further prove our hypothesis that redox reactions could be triggered at relatively low voltage, we explored an alternative label-free approach based on the voltage sensitivity of plasmonic nanostructures[30-34] that would enable us to establish if the particles could act as electrical antennae. To test the effect of low voltage on u-AuNPs, we used a darkfield microscopy to monitor the dynamics of the voltage-modulated intensity of light scattered by the nanoparticles. 125 nm u-AuNPs were immobilized on a glass slide coated with Indium-Tin-Oxide (ITO), which was used as a working electrode in a two-electrode electrochemical cell. u-AuNPs were also used in this experiment as gold surface of the particles needs to be exposed to detect the plasmon resonance, however, slightly bigger particles (125 nm) were used due to limitations in the resolution of the instrument, where each individual pixel corresponds to 200 nm.

A darkfield microscopy image of these u-AuNPs is presented in **Figure 3a**. On application of the electrical potential there is a shift in the plasmon resonance, which is proportional to the charge density. To detect the charge density modulation with high spatial resolution, we then applied a relatively low alternating voltage (0.8 Vpp, 4 Hz). The voltage effect was mapped by computing a fast Fourier transform (FFT) of the time-varying intensity at each pixel. By selecting the

amplitude of the intensity modulation at the frequency of the applied signal (i.e. 4 Hz), a map of the charge density effect is produced as shown in **Figure 3b**. It is worth commenting that these signals are acquired at a scale of 200 nm (i.e. the pixel size). A signal at the single nanoparticle scale (**Figure 3c**) is shown in **Figure 3d**, which confirmed that we could observe intensity modulation at 4 Hz, which corresponds to the frequency of the applied voltage signal. Therefore, it is experimentally confirmed that voltage modulated resonance position is proportional to charge density[31] and this can be used for quantitative imaging of the electric field in a subsequent work.

These results bring out the conclusion that observing localized resonance position modulation on applying a potential difference confirms the accumulation of electrical change around the u-AuNPs at the potential applied. Thus, this supports our early assertion that u-AuNPs are acting as electrical actuators at relatively low voltages.

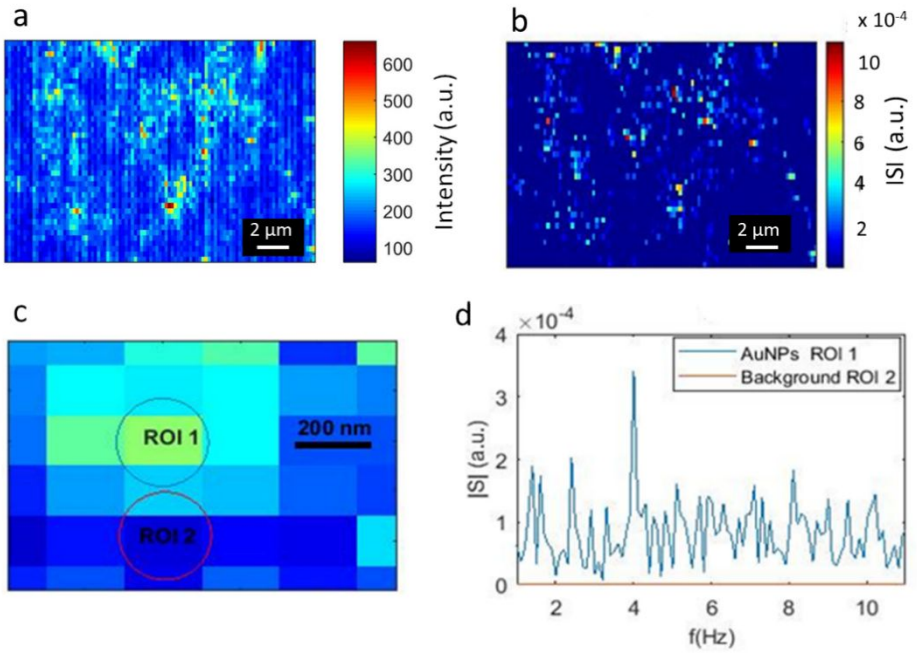

Figure 3. Microscopy images of voltage sensing by plasmonic nanoparticles. (a) A darkfield microscopy images of u-AuNPs; (b) a map of the amplitude of the voltage-modulated scattering intensity (|S|) of 125nm Au nanoparticles, presented to support that low-voltage can be detected by u-AuNPs and therefore can be used as electronic sensors. (c) A magnified view of the darkfield image where the intensity modulation spectrum (d) is obtained.

The objective was to develop a bioelectronic system which would enable us to perform chemical redox reactions, which could be fluorescently monitored, using an external extracellular electrical input. We envisaged based on our earlier results that u-AuNP could be used as intracellular electrical antenna. The particles would then electrically polarize upon application of external extracellular electrical potentials, which could then provide the energy to drive chemistry in a wireless manner. To develop this approach, our strategy was to combine a recently developed surface modification procedure[27] that used a gemini pyridinium based amphiphile (linker) which mediated the incorporation of a Na-ZnTCPP onto ws-AuNPs **(Figure 1b,c)**. These functionalized nanoarticles have previously been shown to be stable for long times[27]. We predicted that Na-ZnTCPP would act as a redox reporter by analysing the changes in its fluorescence[35]. We further wanted to prove that this system could act as a redox reporter when a potential difference is applied, and not as a voltage sensitive dye. We envisaged that by converting the electrical input into an optical output we could electronically communicate with the internal environment of a cell. Others have noted that, on application of voltages at Zn-porphyrin modified electrodes, the redox state of the porphyrin could be modulated[36]; however, this had never been previously achieved in a wireless electrochemical system. To do this, we initially characterised the size of the ws-AuNPs before and after the

incorporation of the Na-ZnTCPP (**Figure 4a**) by DLS. The mean size of the particle was approximately 40 nm before and 60 nm after adding the Na-ZnTCPP. This increase in size of the particles is due to the surface modification of the ws-AuNP, resulting from the electrostatic interactions between the positive charge of the bis-pyridinium salt conforming the shell of the ws-AuNPs and the negative charge of the Na-ZnTCPP after the modification. We also characterized the Na-ZnTCPP modified ws-AuNPs by TEM (**Figure 4b**) which resulted in a mean size of 70 nm.

The steady state absorbance and emission spectra obtained for solutions of free Na-ZnTCPP, ws-AuNPs and Na-ZnTCPP modified ws-AuNPs are shown in **Figure 4c**. Absorbance spectrum of a solution of 1,17 mM Na-ZnTCPP in PBS showed an intense and defined Soret band at 422 nm and two Q bands characteristic of zinc porphyrins[27, 37]. An extremely less intense Soret band is also present in the Na-ZnTCPP modified ws-AuNPs. Solutions containing Na-ZnTCPP modified ws-AuNPs present smaller concentrations of porphyrin than those of free ZnTCPP, corresponding to 1.26 μM Na-ZnTCPP and thus there is a reduction in the intensity of the peak at 422 nm. Regarding the emission spectrum, no observable fluorescent signal was obtained for ws-AuNPs over the wavelength range applied between 550 and 750 nm at λ_{exc} of 420 nm (**Figure 4d**). Peaks in the free Na-ZnTCPP spectrum at approximately 625 nm and 655 nm were observed, respectively. These peaks result from the fluorescence associated with the porphyrin[27, 38], which can also be seen in the emission spectrum of Na-ZnTCPP modified ws-AuNPs. The results obtained from absorption and fluorescence emission spectrum confirms successful modification of ws-AuNPs with Na-ZnTCPP as depicted in **Figure 1**. Moreover, it was noted that the emission

peak ratio was inverted when compared to the free Na-ZnTCPP molecule, which may be attributed to the differing configurations of the electrons when the molecule is bound to the surface[37].

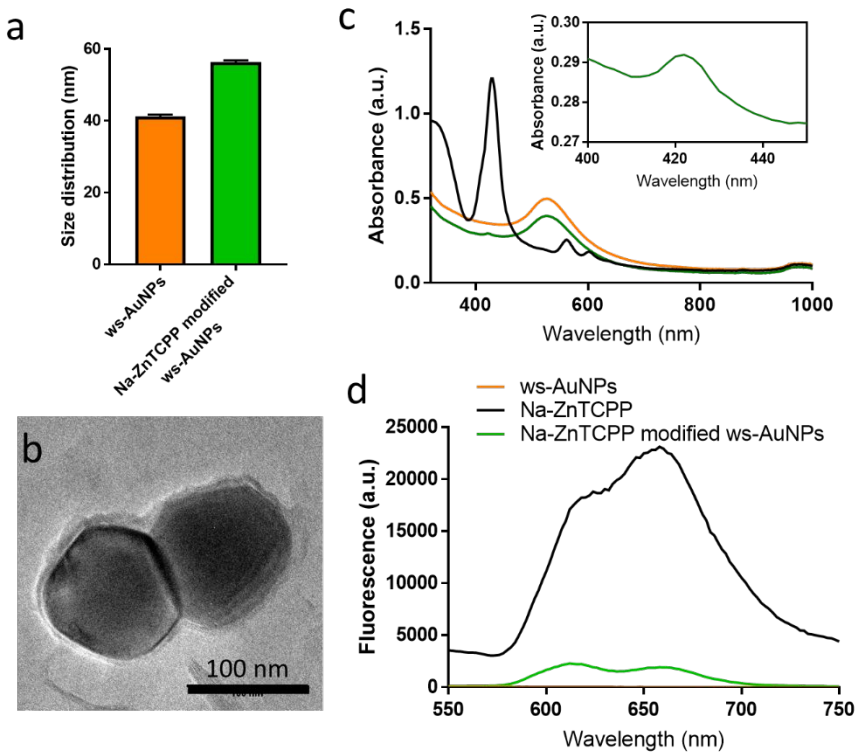

Figure 4. (a) DLS results showing size distribution of ws-AuNPs before and after chemical modification with Na-ZnTCPP (n=3; SD). (b) TEM image of a pair of Na-ZnTCPP modified ws-AuNPs. Scale bar 100 nm. (c) UV-VIS absorbance spectrum and (d) emission spectrum of free Na-ZnTCPP (black), ws-AuNPs (orange) and Na-ZnTCPP modified ws-AuNPs (green).

Before performing intracellular studies, cell uptake of the modified gold nanoparticles was analyzed. In order to test nanoparticle uptake we incubated the Na-ZnTCPP modified ws-AuNPs with a model Chinese Hamster Ovary (CHO) cell line (**Figure 5a**). Additionally, we also wanted to determine the time required for the cells to uptake the nanoparticles to maximize the

concentration inside the cells, and therefore increase the signal to noise ratio of the electronic reporter in the next experiments. Na-ZnTCPP modified ws-AuNPs were incubated with CHO cells at time intervals up to 4 hours and inductively coupled plasma mass spectrometry (ICP-MS) analysis was performed to detect Na-ZnTCPP modified ws-AuNPs. This was performed on samples containing supernatant and samples containing the cell pellet in order to quantify the amount of gold present outside and inside the cells. Incubation with an initial concentration of 100 $\mu g\ L^{-1}$ of Na-ZnTCPP modified ws-AuNPs in Hank's Balanced Salt solution (HBSS) was studied for 4 hours. During this period, the percentage of viable cells was monitored by Trypan blue analysis (**Figure 5b**). The results obtained for ICP-MS analysis can be seen in Figure 5c. On incubations with the cells the concentration of gold in the supernatant was reduced by 27.6 $\mu g\ L^{-1}$ over the 4 hours, whilst the concentration of the gold associated with the cell pellet rose to approximately 26.4 $\mu g\ L^{-1}$-. This provides evidence that the cells were up-taking the Na-ZnTCPP modified ws-AuNPs. Moreover, we quantified the number of Na-ZnTCPP modified ws-AuNPs per cell from the ICP-MS data and found at 30 minutes there were 4, at 1 hours there were 76 and by 4 hours there were approximately 160 nanoparticles per cell (**Figure 5c**). Details of this calculation are given in the methods section.

For future experiments, it appeared that an incubation of 4 hours was suitable for obtaining a higher number of Na-ZnTCPP modified ws-AuNPs per cell, thereby maximizing our signal to noise ratio. It was also important to show that over the 4 hours the cells were viable and there was no detrimental loss in membrane integrity, which could have affected the results of the ICP-MS due to gold nanoparticles leaking from the cells into the supernatant. Consequently, we performed a dye membrane exclusions study in which we incubated Trypan blue with cells exposed to the

Na-ZnTCPP modified ws-AuNPs nanoparticles for up to 4 hours (**Figure 5b**). No difference in membrane viability, and therefore cell death, was observed over the 4 hours suggesting the nanoparticles caused no membrane degradation.

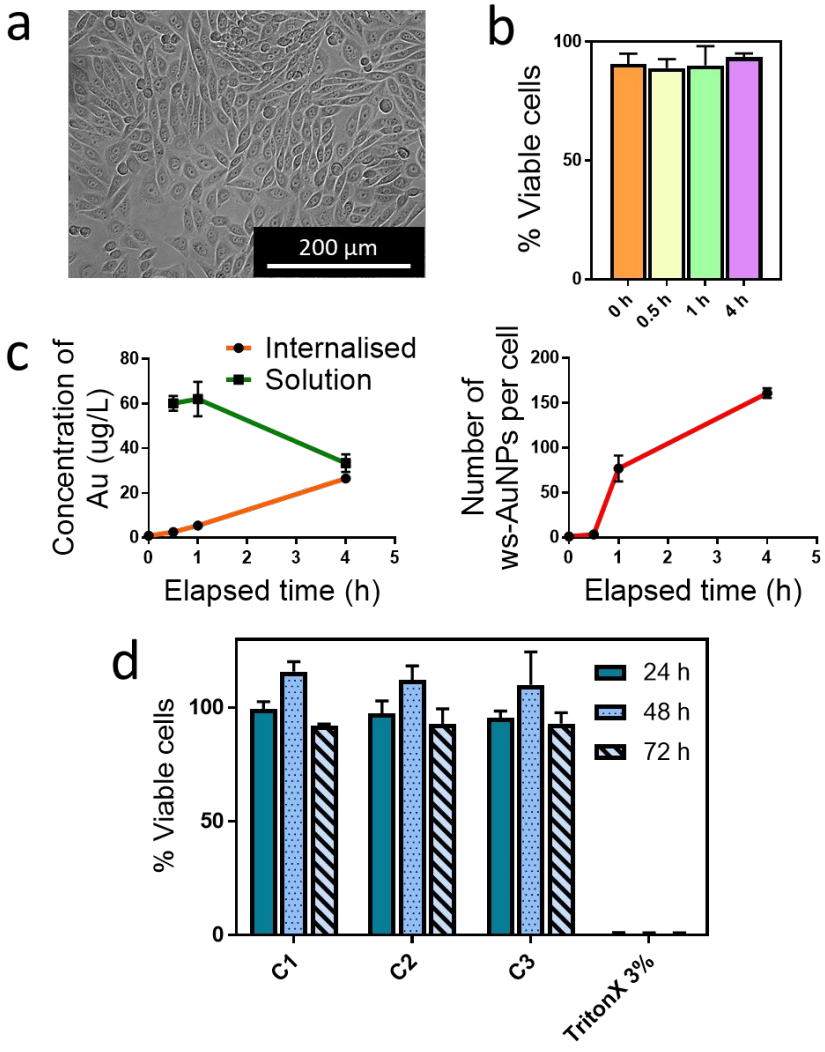

Figure 5. (a) Optical microscopy image of Chinese Hamster Ovary (CHO) cells (scale bar 200 µm). (b) Percentage of viable cells calculated using a trypan blue assay. (c) Inductively coupled plasma mass spectrometry (ICP-MS) analysis of concentration of gold internalized in the cells and in supernatant solution (left) and calculation of gold nanoparticles per cell (right). (d) WST-8

metabolic activity assay of CHO cells incubated with 11.8 μM (C1), 2.36 μM (C2) and 1.18 μM (C3) Na-ZnTCPP modified ws-AuNPs for longer periods of time. TritonX-100 was used as positive control and negative control on cell culture media was assumed as 100% viability. (n=3 ; SD).

The trypan blue exclusion study determined that over 4 hours the nanoparticles caused no cell death; however, the practicality of using such a system long term meant that from this data we could not infer if they were biocompatible on longer time scales. Additionally, the trypan blue cell viability assay does not report on sub-lethal toxic effects. As a result, it was important to assess the effect that the Na-ZnTCPP modified ws-AuNPs had on the cells for longer periods and to use an assay that could report sub-lethal effects such as a metabolic reporter assay. Subsequently the well-known WST-8 metabolic reporter assay[38] was chosen (**Figure 5d**). If cellular metabolism was being perturbed by the nanoparticles, we would expect a drop in cellular metabolism as indicated by the positive control, TritonX-100, which is a widely used toxicant and completely stops cell metabolism. At all the doses investigated, there was no decrease in the absorbance relative to the negative control (culture media only and cells). This indicated that the Na-ZnTCPP modified ws-AuNPs were not inducing detrimental metabolic effects on a longer time scale.

We then proceeded to test our hypothesis that we could electronically communicate with the inside of the cells, via the conductive nanoparticles, by modifying the redox state of the surface bound porphyrins. The relationship between the redox state of Zn porphyrins and their fluorescence emission has been previously studied, it should be possible to switch the fluorescence on and off by controlling the excited-state electron transfer[39-40]. In order to establish if this were

the case, 5-(4-aminophenyl)-10,15,20-(tri-4-sulfonatophenyl)porphyrin triammonium ($TPPS_3$) and its zinc derivative ($ZnTPPS_3$) were covalently linked to gold surfaces. These water-soluble porphyrins possess an analogous chemical structure to Na-ZnTCPP and the presence of the amino group allows for a covalent bond to be formed between carboxylic groups present in gold surfaces after modification with 11-mercaptoundecanoic acid (MUA) and the porphyrins (Figure S6). The presence and absence of the Zn atom in the center of the porphyrin ring could also provide further evidence about the role of this group in the molecule. Characterization of these surfaces can be found in Figure S7. Towards this, changes in fluorescence were measured when cyclic voltammetry (CV) was simultaneously performed which would allow us to assess the effect of redox reactions on the fluorescence.

When CV was performed with $TPPS_3$ modified gold surfaces from 1 V to -0.2 V, it was possible to detect a redox peak at 0.259 V (Figure S8). This did not affect the values of fluorescence as can be seen in **Figure 6a**, where the fluorescence of $TPPS_3$ is not affected by voltage or redox change. On $ZnTPPS_3$ modified gold surfaces a reduction peak was seen at 0.136 V and a broad oxidation signal was observed with a peak at 0.94 V (Figure S8). Since the only difference between molecules is the absence or presence of Zn, we can conclude that this oxidation peak corresponds to the changes in the redox behavior of the porphyrin that results from the inclusion of the Zn atom in the porphyrin ring. Similar results using water soluble zinc porphyrins were reported in the literature, where addition of Zn could increase the irreversibility of the systems[41]. When CV was performed with gold electrodes modified with $ZnTPPS_3$, there is a sharp increase in the value of fluorescence associated to the application of potentials that induce reducing faradaic currents (**Figure 6b**). When an oxidizing potential was reached in the reverse scan after 15 s, there is a

decrease in the values of fluorescence which corresponds to oxidative currents observed. This provides evidence that the fluorescence read out is not due to the dye acting as a voltage sensor but rather a redox sensor. If the molecule was acting as a voltage sensitive dye then we would expect the changes not to align with faradaic processes observed. On the contrary, the fluorescence is altered when redox changes were occurring as seen in the CVs. This indicates that the fluorescence signal of the $ZnTPPS_3$ is linked to the redox state of the porphyrin. Furthermore, changes in the fluorescence of the $ZnTPPS_3$ only take place when the porphyrin is attached to the gold surface. This was not observed when potentials were applied to free $ZnTPPS_3$ (Figure S9).

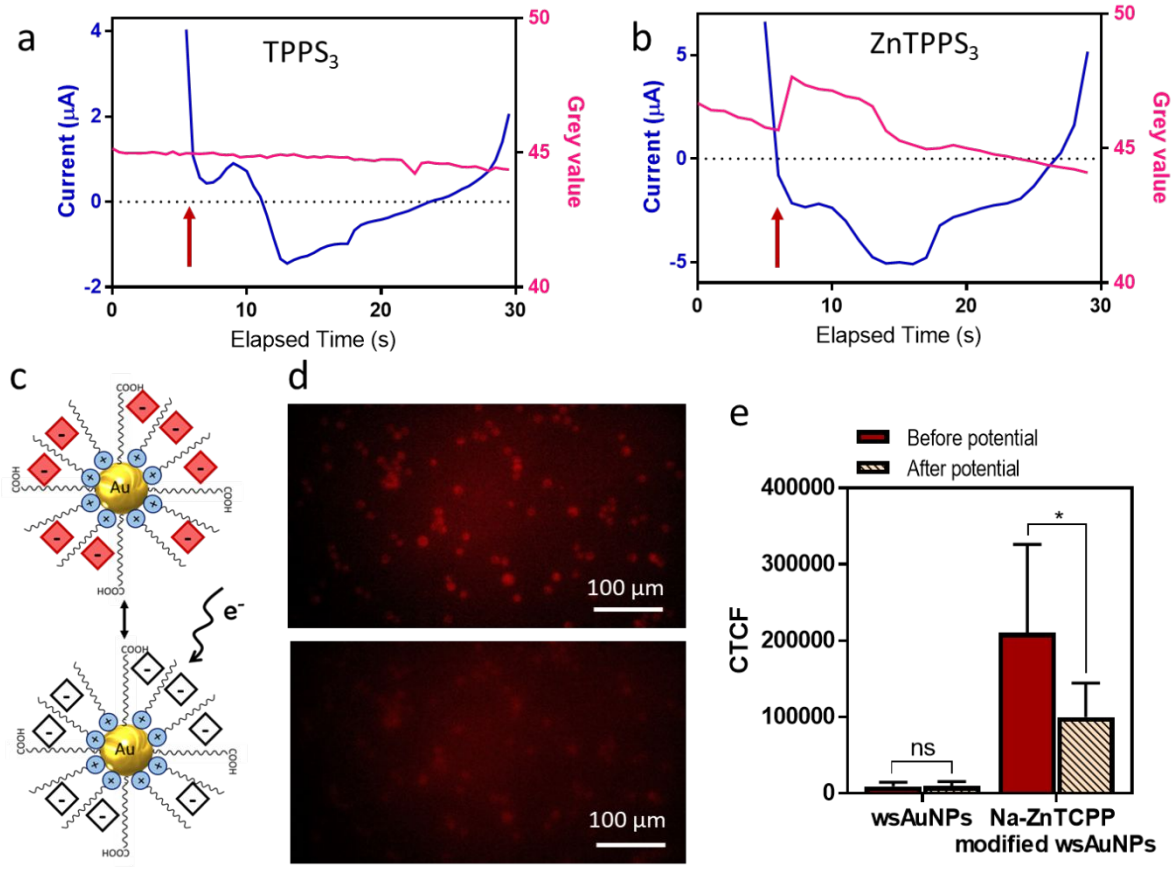

Figure 6. Values of current and grey values measured on (a) $TPPS_3$ and (b) $ZnTPPS_3$ modified gold surfaces when cyclic voltammetry (CV) and fluorescence microscopy was performed

simultaneously. Red arrow indicates when CV was started (start potential 1 V, switching potential -0.2 V vs a Ag/AgCl reference electrode; 100 mV s^{-1}). (c) Diagram showing the result of the application of potentials. Fluorescence microscope images of CHO cells containing Na-ZnTCPP modified ws-AuNPs (d) before application of potentials and (e) after applying the potential. Scale bar 100 μm. (f) Corrected total cell fluorescence quantified in the area of the cells before and after applying the potential. Statistical significance was calculated using a one-way ANOVA test (n=10; SD; *p=0.0117). Scale bar is 100 μm.

We then wanted to establish if the fluorescence could be modulated using external fields when nanoparticles were incubated with cells in a wireless manner. The Na-ZnTCPP modified ws-AuNPs (**Figure 6c**) were incubated with CHO cells for 4 hours to ensure optimal uptake which made them inherently fluorescent, and a sample of cell suspension was placed on the printed electrochemical cell (**Figure 6d**). Due to the electrical properties of cell membranes, acting as resistors and capacitors[42], higher potentials were applied than in earlier wireless studies involving Pd. A potential difference of 150 V was applied between the feeder electrodes while we simultaneously monitored and collected the fluorescence exposed to a 550 nm laser excitation source. To note, this potential is still orders of magnitude smaller than that reported for modulating redox reactions at carbon nanotubes (in the range of kV).

After the application of the potential difference, we observed a reduction in the fluorescence inside the cells (**Figure 6e**). This was confirmed by quantitative measurement of fluorescence intensity of the cells before and after application of potential. Corrected total cell fluorescence

(CTCF) in the area of the cells, calculated by applying the formula in **Equation 1**[43], determined a significant ($P<0.05$) reduction in the fluorescence (**Figure 6f**). Error

associated with the data seen in the CTCF of Na-ZnTCPP modified ws-AuNPs could be due to the background noise level, introducing some variability in the CTCF values. Based on our earlier evidence that redox behavior of the $ZnTPPS_3$ corresponds with changes in fluorescence, we suggest that the mechanism behind the reduction in fluorescence resulting is the oxidation of Na-ZnTCPP. This change was not observed in the controls when incubating the CHO cells with ws-AuNPs, as they do not have the porphyrin **Figure 5F**. Since plain ws-AuNPs do not have the porphyrin group in their composition, they are not as fluorescence and grey values were much lower when compared to ZnTCPP-modified ws-AuNPs (Figure S10). It is also worth noting that on the application of the potential the background noise increases, which is an artefact of the electrochemistry and therefore results in a lower signal noise.

$$Corrected\ total\ cell\ fluorescence = Integrated\ density - (Area\ of\ selected\ cel\ X\ Mean\ fluorescence\ of\ background\ readings \quad \textbf{Eq. 1}$$

This result indicates that changes in fluorescence are mediated by electric field induced redox changes at the intracellular Na-ZnTCPP, as they only occur after the application of external potentials. Integrity of the cell membrane seems to be intact, as cells conserve their round shape after potential application (**Figure 6e**).Thus, this represents a new wireless electronic system, with gold nanoparticles acting as electrical antennae, which then provides the energy to stimulate redox changes at the surface of the nanoparticles. The consequences are that we can intracellularly communicate with the internal environment of the cells via a fluorescent reporter whose redox

state can be altered without the need for any direct electrical contact. It is important to note though, that some bubbles were present in the solution after the application of potentials and it would be desirable in the future to use even lower potentials to avoid this.

Conclusion

In summary, we have shown via electric field redox control of a Pd^{2+} and porphyrin ions, that gold nanoparticles could act as electrical antenna converting electrical input into chemical and fluorescence output. The gold nanoparticles could enter cells and were biocompatible. Once the nanoparticles were inside of the cells, an external electrical stimulus was applied and the nanosensors could convert the electrical input into a chemical change, via Zn-porphyrin redox modulations, to a fluorescence output. This demonstrates the establishment of a generic wireless method to intracellularly communicate electronically with conductive nanoparticles. This will have important implications for future non-invasive sensing and actuating platform that may be used to advance the field of bioelectronics and biosensing.

Materials and methods

Materials

Unless otherwise stated, materials were purchased from Sigma-Aldrich, UK. All the solvents used were reagent grade.

Inkjet printing of an electrochemical cell

An electrochemical cell consisting of two gold feeder electrodes and one silver/silver chloride pseudo reference electrode was inkjet printed. Kapton tape (RS Components, UK) composed of

polyimide was attached to 76 x 26 glass slides (Cole-Palmer) and used as substrates. Glass slides were washed with acetone prior to use. Inks consisted of a silver nanoparticle ink (AgNPink) with an approximate 30% of solid content purchased from ANP Ltd, and a gold nanoparticle ink (AuNPink) containing 12% of solid content (Printed Electronics Ltd., Tamworth, UK).

Inks were filtrated (HPLC Nylon 5.0 μm syringe filters, Cole-Parmer) and injected into the propylene print cartridge (DMC-11610, 10 pl and DMCLCP-11610), which were fixed to the printhead prior to printing, on a piezo electric drop-on-demand Dimatix Materials Printer (Model DMP-2800, FUJIFILM Dimatix, Inc. Santa Clara, CA). Printheads had 16 jetting nozzles (21 μm in diameter). Bit-maps of patterns were developed by GNU Image Manipulation Program (version 2.8.16) and adapted using the Dimatix materials printer software. Patterns were printed by jetting 846 drops per inch (DPI), corresponding to a drop spacing of 30 μm, and using custom print waveforms. Single nozzles were used to improve the resolution of the patterns and avoid the formation of clogs. When printing, the temperature was set and held to 100°C using a custom-built heater inside the printer. Firing voltages varied over a range of 20-25 V to allow an optimal speed of ink droplet ejection from the nozzles. Sintering of nanoparticles was carried out in an oven at 150°C and 250°C for an hour for the AgNPink and the AuNPink respectively. Three layers of AgNPink and five layers of AuNPink were printed.

Testing of printed electrochemical cell was carried out at room temperature using a VersaSTAT 4 potentiostat interfaced with a personal computer and integrated with VersaStudio Software (Princeton Applied Research). The supporting electrolyte was phosphate buffer saline (PBS) dissolved in deionized water (0.01 M phosphate buffer, 0.0027 M potassium chloride and 0.137

M sodium chloride), 1 mM potassium hexacyanoferrate (III) in PBS was used as the electroactive species. Potentials are reported vs. an inkjet Ag pseudoreference electrode. Printed gold feeder electrodes were used as working and auxiliary electrodes. Cyclic voltammograms (CVs) were acquired when a potential was applied from 0.8 V to -0.3 V at a scan rate of 5 mV s^{-1}.

Electrodeposition of palladium onto unmodified gold nanoparticles (u-AuNPs)

50 nm unmodified PBS stabilized gold nanoparticles (u-AuNPs), giving an optical density of 1, stabilized in 0.1 mM PBS and reactant free were used as bipolar electrodes within the printed cell, where the gap between gold feeder electrodes was 210 μm. A solution of 1 mM $PdCl_2$ in PBS was added to the dispersion of u-AuNPs. 20 μl of this suspension were placed in contact with all the elements of the system. Chronoamperometry was performed with the aforementioned instrument. 10 V were applied for varying times of 1, 5 and 15 minutes.

Size characterization of the u-AuNPs dispersion was carried out by Dynamic Light Scattering (DLS) using a Malvern zetasizer Nano ZS (Malvern Instruments, UK) after the electrodeposition. TEM sample preparation was performed by placing 15 μL of the sample of u-AuNPs + 1 mM $PdCl_2$ without stimulation and stimulated at 10 V for 10 minutes on a carbon coated copper grid (400 Mesh, Agar Scientific), the sample was allowed to sit on the grid for at least 3 h before imaging. Morphology and EDX analysis was carried out using a transmission electron microscope (JEOL 2000 FX TEM) equipped with Oxford Instruments XMax 80 INCA EDS system, operating at 200 kV accelerating voltage. Scanning Electron Microscopy (SEM) was used on a FEI Quanta 650 SEM to examine the morphology of the deposits. The sample preparation required the deposition of the suspensions into a holey carbon Transmission Electron Microscopy (TEM) grid.

Visualization of the nanoparticles was carried out in FEI Quanta 650 SEM. Elemental mapping results were performed with an energy-dispersive X-ray spectrometer (EDX) incorporated in the SEM.

In order to discard pH-induced aggregation, solutions were incubated in either PBS (pH 7.4 at 25^{o}C), a commercial buffer solution at pH 4 ± 0.01 at 20^{o}C (SLS Select) and a commercial buffer solution at pH 2 ± 0.02 at 25^{o}C (Reagecon). Size of particles was measured by DLS after 1 and 15 minutes. pH of the system was also monitored for 15 minutes when the potentials were applied and measured on a pH meter (Metler Toledo).

Plasmonic-based detection of electrical charge modulation at u-AuNPs

A darkfield microscopy setup was used to image the voltage effect on the u-AuNPs. In this setup, the sample was illuminated with a 633 nm collimated light. The sample plane was imaged on CMOS camera (SV643M, Epix) to collect the forward-scattered light by nanoparticles. To study the low voltage effect on 125 nm u-AuNPs (Nanopartz Inc.), an electrostatic layer-by-layer self-assembly process was used to bond the particles to a conducting substrate to avoid being washed out while serving as a working electrode. Firstly, a layer of potassium hydroxide (KOH) solution was deposited for 1 hour on a glass cover-slip coated with 10 nm of Indium-Tin-Oxide (ITO). Then, two synthetic polymers, poly(allylamine hydrochloride) (PAH) and poly(sodium 4-styrenesulfonate) (PSS), were deposited for 30 minutes each. Between all these steps, the substrate was washed with deionized water and dried with nitrogen. Once the polymer layers were completed, 50 µl of a solution of u-AuNPs (125 nm diameter) with a concentration of 1.47E9 NPs/ml was drop-coated and dried overnight. For sensitive detection of the voltage effect, the

wavelength and the particle size and shape must be carefully selected. Here, the wavelength of 633 nm is located at the highest gradient of the scattering spectrum of the 125 nm u-AuNPs, in aqueous solution, where maximum change in scattering due to the applied voltage is obtained. A sinusoidal voltage modulation with 0.8 Vpp at 4 Hz was applied to the substrate-integrated nanoparticles, against a platinum reference electrode, while recording modulation of light scattering simultaneously using CMOS camera (SV643M, Epix, Buffalo Grove, IL, USA) with 100 Hz sampling frequency. To map the voltage effect on the u-AuNPs, a fast Fourier transform (FFT) of the dynamic scattering intensity was computed for each pixel. The map was produced by selecting the amplitude of the voltage-modulated intensity at the frequency of the applied signal.

Synthesis and characterization of water-soluble gold nanoparticles (ws-AuNPs)

Details about synthesis and characterization were described elsewhere. Measurements of absorbance and emission spectra were performed on a Tecan microplate reader. Absorbance was scanned form 200 nm-1000 nm at room temperature with a wavelength step size of 2 nm of solutions of 1.17 mM of a Zn(II)meso-tetrakis(4-carboxylatephenyl)porphyrin sodium salt (Na-ZnTCPP), and 2.77 μM ws-AuNPs with and without Na-ZnTCPP in PBS. Emission spectra of the previous solutions was measured from 550 nm to 750 nm at an excitation wavelength of 420 nm at room temperature. A 10 μl drop of Na-ZnTCPP modified ws-AuNPs dispersion was deposited on a TEM carbon-coated copper grid (Agar Scientific) and dried at room temperature before measurements. TEM measurements were performed on a Jeol 2100 Plus TEM at an accelerating voltage of 80 kV.

Cell culture

Chinese Hamster Ovary (CHO) cells were cultured in corning T-75 cm^2 flasks in 15 ml of media supplemented with 10% fetal bovine serum (FBS), 2.4% HEPES buffer solution and 1% penicillin/streptomycin for 2-3 days in an incubator at 37°C in 5% CO_2 atmosphere and passaged with trypsin when 70 – 80 % confluent.

Uptake of Na-ZnTCPP modified ws-AuNPs was analyzed by inductively coupled plasma mass spectrometry (ICP-MS). Approximately 1.50×10^3 cells were reseeded on 6 well-plates 48 hours before experiments. Na-ZnTCPP modified ws-AuNPs were added at a final concentration of 2.54 μM in Hank's Balanced Salt solution (HBSS) and incubated for 0.5, 1 and 4 hours. After each time point, solution was collected, centrifuged at 4000 rpm for 5 minutes and pellet saved for ICP-MS analysis. Cells were rinsed three times with PBS and trypsinized and collected in a Falcon tube. 10 μl of cell suspension were mixed with trypan blue in a ratio 1:1 and counted on a haemocytometer after each time point. Well plates were washed with 10% FBS in HBSS solution and collected with the cell's prior centrifugation at 1200 rpm for 5 minutes. Pellets containing the cells were saved for ICP-MS analysis. Solutions were digested in 5% aqua regia (trace metal grade HCl and HNO_3 in a proportion of 3:1) and left overnight. After digestion, solutions were diluted to reach a final concentration of acid of 2%, filtered and collected for analysis on an iCAPQ Thermo Fischer inductively coupled plasma mass spectrometer. Standard solutions were used to develop a calibration curve. The number of nanoparticles per cell was calculated by firstly gaging the number of Au atoms present in the 50 nm nanoparticles assuming a crystalline structure. This allows us to know the mass of Au per nanoparticle and compare it to ICP-MS results to obtain the total number of particles in each sample. The cells were counted as described earlier; we can then calculate the number of particles per cell at the different time points.

Biocompatibility studies for longer incubation times were performed using a water-soluble tetrazolium salt (WST-8) assay. 7500 cells were incubated on 96 well plates 24 hours prior experiment. Na-ZnTCPP modified ws-AuNPs at different concentrations were added (C1: 11.8 μM, C2: 2.36 μM and C3: 1.18 μM) and incubated with cells for 24, 48 and 72 hours. After each incubation time, media was replaced with 10% WST-8 in complete DMEM and incubated for an hour before reading absorbance at 450 nm in a Tecan microplate reader. Controls (culture media as negative control and TritonX-100 3% as positive control) and blanks were used. Values are presented relative to negative controls.

Detection of fluorescence of modified gold surfaces during cyclic voltammetry

Thermally deposited gold glass slides (Georg-Albert PVD) were cleaned by immersing them into a solution of 50 mM KOH and 25% H_2O_2 for 10 min followed by rinsing with Milli-Q water prior chemical modification. Carboxylic groups were introduced on the gold electrodes by submerging them in 2 mM solution of 98% 11-mercaptoundecanoic acid (MUA) in ethanol for 48 h followed by multiple washes with ethanol and MilliQ water. For the covalent attachment of 5-(4-aminophenyl)-10,15,20-(tris-4'-sulfonatophenyl)porphyrin triammonium ($TPPS_3$) and Zinc (II)5-(4-aminophenyl)-10,15,20-(tris-4'-sulfonatophenyl)porphyrin triammonium ($ZnTPPS_3$) (Porphychem, France), the MUA functionalized gold electrodes were submerged in a 40 mM aqueous solution of EDC and 10 mM NHS for 2 h. Afterwards the gold electrodes were immediately transferred to a 200 μM aqueous solution of $TPPS_3$ and Zn $TPPS_3$ and kept for 24 h. Samples were thoroughly washed with MilliQ water and dried with nitrogen.

Characterization of surface modification on gold surface was performed by water contact angle using a CAM 200 optical contact angle meter from KSV Instruments ltd. Oneattenuation software was used analyse the contact angle of a water droplet generated from a micro syringe at the three-phase interaction. Average contact angles and standard deviation were determined by analysing three different areas of each surface in triplicate. The thickness of the bound monolayers were determined measured with a J.A. Woollam Co., Inc., spectroscopic ellipsometer α-SE and equipped with CompleteEASE software. A wavelength range of 300-800 nm was used with a fixed angle of incidence (70°). The Ellipsometry model was based on multiple layers, three-phase ambient/SAM/Au. Average thickness and standard deviation were determined by analysing three different areas of each surface in triplicate.

Changes in fluorescence of modified gold surfaces were monitored using a Nikon ECLIPSE TE300 fluorescent microscope equipped with a QImaging optiMOS, Scientific CMOS camera. Modified gold surfaces were transferred to a 6-well plate containing PBS and positioned in the microscope stage where fluorescence signal was monitored. Cyclic voltammetry was simultaneously performed using a MetrOhm Autolab potentiostat incorporated with NOVA software. Gold surfaces were used as working electrode and a platinum wire in contact with the solution closed the circuit and was used as counter electrode. A Ag/AgCl electrode was used as reference. Initial potential was 1 V and switching potential was -0.2 V. Scan rate was 100 mV s^{-1}. All measurements were performed in PBS vs a Ag/AgCl reference electrode. ImageJ 1.52a open source software was used to perform image analysis and determination of grey values. Three different videos of each type of porphyrin were analyzed.

Intracellular wireless actuation

CHO cells were incubated at a concentration of 1.50×10^3 cells per well on a 6-well plate 48 hours prior experiments. 2.54 μM of Na-ZnTCPP modified ws-AuNPs and plain ws-AuNPs, were incubated for 4 hours and cells were suspended using trypsine. 20 μl of suspension containing cells was placed between gold feeder electrodes and 150 V were applied using an in-house-made voltage power supply. 550 nm laser was used as excitation source. Fluorescence images were obtained using the previous method. Quantification of the corrected total cell fluorescence was calculated in ImageJ. Statistical significance was calculated using a one-way ANOVA test on 10 cells per sample on Graphpad Prism 7.01.

ASSOCIATED CONTENT

Supporting Information.

The following files are available free of charge.

Supporting figures of design, dimensions and functionality test of inkjet printed electrochemical cell, TEM and EDX spectra of u-AuNPs + 1 mM $PdCl_2$ with and without electrical stimulation, SEM and EDX elemental mapping of u-AuNPs + 1 mM $PdCl_2$ after potential application, mechanism of chemical modification of gold surfaces with Zn porphyrins, characterization of modified gold surfaces, and fluorescence microscopy images of CHO cells with ws-AuNPs (.DOC).

AUTHOR INFORMATION

Corresponding Author

*E-mail: Frankie.Rawson@nottingham.ac.uk Tel.: (+44) 0115 84698

Author Contributions

PSA performed inkjet printing of electrodes, electrochemical experiments, characterization experiments on u-AuNPs and ws-AuNPs and wireless intracellular sensing. AJ performed the surface modification with Zn-$TPPS_3$ and $TPPS_3$, and their characterization and TEM imaging of u-AuNPs. AJS performed the sample preparation of u-AuNPs with and without electrical stimulation for TEM imaging. SAA concept, instrumentation design and signal processing of plasmonic imaging, SAA and RFD performed the plasmonic measurements. MEAR and LPG performed the synthesis and preliminary characterization of ws-AuNPs and Na-ZnTCPP. PSA, SAA and FJR wrote the manuscript. PSA, AJ, MRA, RJMH, LPG and FJR discussed the experimental design and results. All the authors read, commented and approved the final manuscript.

Funding Sources

This work was supported by the Engineering and Physical Sciences Research Council EP/R004072/1, EP/K005138/1, E0P/M50810X/1 and EU ERDF (FEDER) funds and MINECO through the Spanish Government (TEC2017-85059-C3-2-R). We thank the BBSRC (BB/L017059/1) and Leverhulme Trust (ECF/2013-603) for financial support. The University of Nottingham for funding the Nottingham Research

Fellowship currently held by Dr Rawson and the Anne McLaren Research Fellowship held by Dr. Perez-Garcia.

ACKNOWLEDGMENT

Prof Alexander Kuhn is thanked for insightful discussion. Dr. Scott Young and Dr. Saul Vazquez-Reina are thanked for their assistance with ICP-MS analysis. Dr. Marion Limo is thanked for help provided for TEM analysis. Dr. Nigel Neate and Dr. Michael Fey are thanked for assistance on TEM and SEM analysis, respectively. The authors thank the Nanoscale and Microscale Research Centre (nmRC) for providing access to instrumentation.

ABBREVIATIONS

Chinese Hamster Ovary cells, CHO cells; Corrected total cell fluorescence, CTCF; Cyclic Voltammetry, CV; Dynamic light scattering, DLS; Energy dispersive X-ray, EDX; Fast Fourier transform, FFT; Hank's balanced salt solution, HBSS; Indium-tin-oxide, ITO; Inductively coupled plasma mass spectrometry, ICP-MS; Scanning electron microscopy, SEM; Sodium tetrakis(4-carboxyphenyl)porphyrin, Na-H_2TCPP; Sodium Zn(II)meso-tetrakis(4-carboxylatephenyl)porphyrin, Na-ZnTCPP; Transmission electron

microscopy,TEM; Unmodified gold nanoparticles , u-AuNPs; Water-soluble gold nanoparticles, ws-AuNPs; Water-soluble tetrazolium salt, WST-8.

REFERENCES

1. Famm, K.; Litt, B.; Tracey, K. J.; Boyden, E. S.; Slaoui, M., Drug Discovery: a Jump-Start for Electroceuticals. *Nature* **2013**, *496* (7444), 159-161.
2. Birmingham, K.; Gradinaru, V.; Anikeeva, P.; Grill, W. M.; Pikov, V.; McLaughlin, B.; Pasricha, P.; Weber, D.; Ludwig, K.; Famm, K., Bioelectronic Medicines: a Research Roadmap. *Nat Rev Drug Discov* **2014**, *13* (6), 399-400.
3. Sanjuan-Alberte, P.; Rawson, F. J., Engineering the Spark into Bioelectronic Medicine. *Fut Sci* **2019**, *10* (3), 139-142.
4. Sanjuan-Alberte, P.; Alexander, M. R.; Hague, R. J. M.; Rawson, F. J., Electrochemically Stimulating Developments in Bioelectronic Medicine. *Bioelec Med* **2018**, *4* (1), 1.
5. Rawson, F. J.; Cole, M. T.; Hicks, J. M.; Aylott, J. W.; Milne, W. I.; Collins, C. M.; Jackson, S. K.; Silman, N. J.; Mendes, P. M., Electrochemical Communication with the inside of Cells using Micro-Patterned Vertical Carbon Nanofibre Electrodes. *Sci Rep* **2016**, *6*, 37672.
6. Rawson, F. J.; Hicks, J.; Dodd, N.; Abate, W.; Garrett, D. J.; Yip, N.; Fejer, G.; Downard, A. J.; Baronian, K. H. R.; Jackson, S. K., Fast, Ultrasensitive Detection of Reactive Oxygen Species using a Carbon Nanotube Based-Electrocatalytic Intracellular Sensor. *ACS Appl. Mater. Interf.* **2015**, *7* (42), 23527-23537.
7. Rawson, F. J.; Yeung, C. L.; Jackson, S. K.; Mendes, P. M., Tailoring 3D Single-Walled Carbon Nanotubes Anchored to Indium Tin Oxide for Natural Cellular Uptake and Intracellular Sensing. *Nano Lett* **2012**, *13* (1), 1-8.
8. Qing, Q.; Jiang, Z.; Xu, L.; Gao, R.; Mai, L.; Lieber, C. M., Free-Standing Kinked Nanowire Transistor Probes for Targeted Intracellular Recording in Three Dimensions. *Nat Nanotechnol* **2014**, *9* (2), 142-147.
9. Zhang, A.; Lieber, C. M., Nano-Bioelectronics. *Chem Rev* **2016**, *116* (1), 215-257.
10. Actis, P.; Tokar, S.; Clausmeyer, J.; Babakinejad, B.; Mikhaleva, S.; Cornut, R.; Takahashi, Y.; Lopez Cordoba, A.;

Novak, P.; Shevchuck, A. I.; Dougan, J. A.; Kazarian, S. G.; Gorelkin, P. V.; Erofeev, A. S.; Yaminsky, I. V.; Unwin, P. R.; Schuhmann, W.; Klenerman, D.; Rusakov, D. A.; Sviderskaya, E. V.; Korchev, Y. E., Electrochemical Nanoprobes for Single-Cell Analysis. *ACS Nano* **2014**, *8* (1), 875-84.
11. Wang, Y.; Noel, J. M.; Velmurugan, J.; Nogala, W.; Mirkin, M. V.; Lu, C.; Guille Collignon, M.; Lemaitre, F.; Amatore, C., Nanoelectrodes for Determination of Reactive Oxygen and Nitrogen Species inside Murine Macrophages. *Proc Natl Acad Sci U S A* **2012**, *109* (29), 11534-9.
12. Lee, D.; Lee, D.; Won, Y.; Hong, H.; Kim, Y.; Song, H.; Pyun, J.; Cho, Y. S.; Ryu, W.; Moon, J., Insertion of Vertically Aligned Nanowires into Living Cells by Inkjet Printing of Cells. *Small* **2016**, *12* (11), 1446-1457.
13. Liu, J.; Xie, C.; Dai, X.; Jin, L.; Zhou, W.; Lieber, C. M., Multifunctional Three-Dimensional Macroporous Nanoelectronic Networks for Smart Materials. *Proc Natl Acad Sci U S A* **2013**, *110* (17), 6694-9.
14. Sanjuan-Alberte, P.; Saleh, E.; Shaw, A. J.; Lacalendola, N.; Willmott, G.; Vaithilingam, J.; Alexander, M. R.; Hague, R. J. M.; Rawson, F. J., Remotely Controlled in Situ Growth of Silver Microwires Forming Bioelectronic Interfaces. *ACS Appl Mater Interfaces* **2019**, *11* (9), 8928-8936.
15. Sanjuán-Alberte, P.; Abayzeed, S. A.; Fuentes-Domínguez, R.; Alea-Reyes, M. E.; Clark, M.; Hague, R. J. M.; Alexander, M. R.; Pérez-García, L.; Rawson, F. J., *Wireless Bioelectronic Nanosystems for Intracellular Communication*. 2018.
16. Loget, G.; Kuhn, A., Electric Field-Induced Chemical Locomotion of Conducting Objects. *Nat Commun* **2011**, *2*, 535.
17. Loget, G.; Roche, J.; Kuhn, A., True Bulk Synthesis of Janus Objects by Bipolar Electrochemistry. *Adv Mater* **2012**, *24* (37), 5111-5116, 5144.
18. Fosdick, S. E.; Knust, K. N.; Scida, K.; Crooks, R. M., Bipolar Electrochemistry. *Angew Chem Intern Ed* **2013**, *52* (40), 10438-10456.
19. Warakulwit, C.; Nguyen, T.; Majimel, J.; Delville, M. H.; Lapeyre, V.; Garrigue, P.; Ravaine, V.; Limtrakul, J.; Kuhn, A., Dissymmetric Carbon Nanotubes by Bipolar Electrochemistry. *Nano Lett* **2008**, *8* (2), 500-4.
20. Loget, G.; Kuhn, A., Shaping and exploring the micro- and nanoworld using bipolar electrochemistry. *Anal Bioanal Chem* **2011**, *400* (6), 1691-1704.
21. Casal-Dujat, L.; Rodrigues, M.; Yague, A.; Calpena, A. C.; Amabilino, D. B.; Gonzalez-Linares, J.; Borras, M.; Perez-Garcia, L., Gemini Imidazolium Amphiphiles for the Synthesis, Stabilization, and Drug Delivery from Gold Nanoparticles. *Langmuir* **2012**, *28* (5), 2368-81.

22. Penon, O.; Patino, T.; Barrios, L.; Nogues, C.; Amabilino, D. B.; Wurst, K.; Perez-Garcia, L., A new Porphyrin for the Preparation of Functionalized Water-Soluble Gold Nanoparticles with Low Intrinsic Toxicity. *ChemistryOpen* **2015**, *4* (2), 127-36.
23. Alkilany, A. M.; Thompson, L. B.; Boulos, S. P.; Sisco, P. N.; Murphy, C. J., Gold Nanorods: Their Potential for Photothermal Therapeutics and Drug Delivery, Tempered by the Complexity of their Biological Interactions. *Adv Drug Deliv Rev* **2012**, *64* (2), 190-199.
24. Dreaden, E. C.; Alkilany, A. M.; Huang, X.; Murphy, C. J.; El-Sayed, M. A., The Golden Age: Gold Nanoparticles for Biomedicine. *Chem Soc Rev* **2012**, *41* (7), 2740-79.
25. Giljohann, D. A.; Seferos, D. S.; Daniel, W. L.; Massich, M. D.; Patel, P. C.; Mirkin, C. A., Gold Nanoparticles for Biology and Medicine. *Angew Chem Int Ed Engl* **2010**, *49* (19), 3280-94.
26. Elahi, N.; Kamali, M.; Baghersad, M. H., Recent Biomedical Applications of Gold Nanoparticles: A Review. *Talanta* **2018**, *184*, 537-556.
27. Alea-Reyes, M. E.; Soriano, J.; Mora-Espi, I.; Rodrigues, M.; Russell, D. A.; Barrios, L.; Perez-Garcia, L., Amphiphilic Gemini Pyridinium-Mediated Incorporation of Zn(II)meso-tetrakis(4-carboxyphenyl)porphyrin into Water-Soluble Gold Nanoparticles for Photodynamic Therapy. *Colloid Surf B Biointerf* **2017**, *158*, 602-609.
28. Rasmussen, M.; Serov, A.; Artyushkova, K.; Chen, D.; Rose, T. C.; Atanassov, P.; Harris, J.; Minteer, S., Enhancement of Electrocatalytic Oxidation of Glycerol by Plasmonics. *Chem ElectroChem* **2018**, *6* (1), 241-145.
29. Di Martino, G.; Turek, V. A.; Lombardi, A.; Szabó, I.; de Nijs, B.; Kuhn, A.; Rosta, E.; Baumberg, J. J., Tracking Nanoelectrochemistry using Individual Plasmonic Nanocavities. *Nano Lett* **2017**, *17* (8), 4840-4845.
30. Zhou, H.; Liu, Q.; Rawson, F. J.; Ma, W.; Li, D. W.; Li, D.; Long, Y. T., Optical Monitoring of Faradaic Reaction using Single Plasmon-Resonant Nanorods Functionalized with Graphene. *Chem Comm* **2015**, *51* (15), 3223-3226.
31. Abayzeed, S. A.; Smith, R. J.; Webb, K. F.; Somekh, M. G.; See, C. W., Sensitive Detection of Voltage Transients using Differential Intensity Surface Plasmon Resonance System. *Opt Express* **2017**, *25* (25), 31552-31567.
32. Jing, C.; Rawson, F. J.; Zhou, H.; Shi, X.; Li, W. H.; Li, D. W.; Long, Y. T., New Insights into Electrocatalysis Based on Plasmon Resonance for the Real-Time Monitoring of Catalytic Events on Single Gold Nanorods. *Anal Chem* **2014**, *86* (11), 5513-5518.

33. Huang, Y.; Pitter, M. C.; Somekh, M. G., Morphology-Dependent Voltage Sensitivity of a Gold Nanostructure. *Langmuir* **2011**, *27* (22), 13950-61.
34. Huang, Y.; Pitter, M. C.; Somekh, M. G., Time-Dependent Scattering of Ultrathin Gold Film under Potential Perturbation. *ACS Appl Mater Interfaces* **2012**, *4* (8), 3829-36.
35. Xiao, X. W.; Xu, W.; Zhang, D. Q.; Xu, H.; Lu, H. Y.; Zhu, D. B., A new Fluorescence-Switch based on Supermolecular Dyad with (tetraphenylporphyrinato) zinc(II) and tetrathiafulvalene Units. *J Mater Chem* **2005**, *15* (26), 2557-2561.
36. Lahav, M.; Gabriel, T.; Shipway, A. N.; Willner, I., Assembly of a Zn (II)-Porphyrin– Bipyridinium Dyad and Au-Nanoparticle Superstructures on Conductive Surfaces. *J Am Chem Soc* **1999**, *121* (1), 258-259.
37. Apanasovich, V. V.; Novikov, E. G.; Yatskov, N. N.; Koehorst, R. B. M.; Schaafsma, T. J.; Van Hoek, A., Study of the Zn-Porphyrin Structure by Fluorescence Spectroscopy Methods. *J Appl Spectrosc* **1999**, *66* (4), 613-616.
38. Tominaga, H.; Ishiyama, M.; Ohseto, F.; Sasamoto, K.; Hamamoto, T.; Suzuki, K.; Watanabe, M., A Water-Soluble Tetrazolium Salt useful for Colorimetric Cell Viability Assay. *Anal Commun* **1999**, *36* (2), 47-50.
39. Norel, L.; Tourbillon, C.; Warnan, J.; Audibert, J. F.; Pellegrin, Y.; Miomandre, F.; Odobel, F.; Rigaut, S., Redox-Driven Porphyrin based Systems for new Luminescent Molecular Switches. *Dalton Trans* **2018**, *47* (25), 8364-8374.
40. Rochford, J.; Rooney, A. D.; Pryce, M. T., Redox Control of Meso-Zinc(II) Ferrocenylporphyrin based Fluorescence Switches. *Inorg Chem* **2007**, *46* (18), 7247-9.
41. Neumann-Spallart, M.; Kalyanasundaram, K., On the One and Two-Electron Oxidations of Water-Soluble Zinc Porphyrins in Aqueous Media. *Z Naturforsch B* **1981**, *36* (5), 596-600.
42. Goldman, D. E., Potential, Impedance, and Rectification in Membranes. *J Gen Physiol* **1943**, *27* (1), 37-60.
43. Gavet, O.; Pines, J., Progressive Activation of CyclinB1-Cdk1 Coordinates Entry to Mitosis. *Dev Cell* **2010**, *18* (4), 533-43.

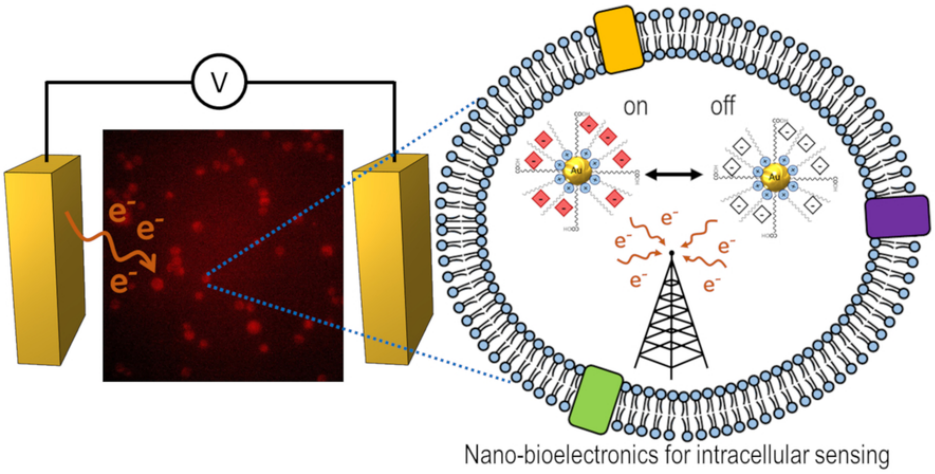

TOC image

79x39mm (300 x 300 DPI)